

# Active Design of Diffuse Acoustic Fields in Enclosures

Wilkins Aquino,<sup>1, a</sup> Jerry Rouse,<sup>2</sup> and Marc Bonnet<sup>3</sup>

<sup>1</sup>*Department of Mechanical Engineering and Materials Science, Duke University, Durham. NC, 27708, USA*

<sup>2</sup>*Analytical Structural Dynamics, Sandia National Laboratories, Albuquerque, New Mexico, 87123, USA*

<sup>3</sup>*POEMS (CNRS-ENSTA-INRIA), ENSTA Paris, Palaiseau, France*

1 This paper presents a numerical framework for designing diffuse fields in rooms of  
2 any shape and size, driven at arbitrary frequencies. That is, we aim at overcoming  
3 the Schroeder frequency limit for generating diffuse fields in an enclosed space. We  
4 formulate the problem as a Tikhonov regularized inverse problem and propose a low-  
5 rank approximation of the spatial correlation that results in significant computational  
6 gains. Our approximation is applicable to arbitrary sets of target points and allows  
7 us to produce an optimal design at a computational cost that grows only linearly  
8 with the (potentially large) number of target points. We demonstrate the feasibility  
9 of our approach through numerical examples where we approximate diffuse fields at  
10 frequencies well below the Schroeder limit.

---

<sup>a</sup>[wilkins.aquino@duke.edu](mailto:wilkins.aquino@duke.edu)

## 11 I. INTRODUCTION

12 Many aerospace structures, satellites and internal components experience acoustic loads  
13 that are diffuse in nature. That is, these loads are composed of a large number of waves  
14 having random amplitude, propagation direction and phase. Ground-based qualification  
15 testing of these structures are typically performed in acoustic reverberation chambers within  
16 which a diffuse field arises naturally. The minimum frequency beyond which an acoustic  
17 field in an enclosure is (naturally) diffuse, termed the Schroeder frequency<sup>1,2</sup>, depends on  
18 the chamber volume  $V$  and absorption as per the relation

$$f_s = \sqrt{\frac{c^3 T_{60}}{4 \ln(10)V}} \quad (1)$$

19 Here,  $c$  is the phase speed and  $T_{60}$  the reverberation time, the time required after source  
20 termination for the energy in the room to attenuate 60 dB. This expression provides an  
21 estimate of the frequency at which sufficient modal overlap first occurs. See Kuttruff<sup>3</sup> for a  
22 detailed derivation of (1).

23 The dimensions of a chamber determine the lowest frequency at which a diffuse field  
24 would naturally occur, as  $f_s^2$  is inversely proportional to the enclosure volume. Although  
25 there are means to improve or fully develop a diffuse field within a given chamber such as  
26 splayed walls, rotating panels, and moving vanes<sup>4</sup>, there are currently no known means to  
27 induce a diffuse field at frequencies below  $f_s$ .

28 Traditionally, large air horns were used to generate the necessary high amplitude acoustic  
29 levels within reverberation chambers. Recently, horns have been augmented or replaced  
30 with concert-grade loudspeakers, allowing improved closed-loop control and the potential

31 to achieve a wider range of test spectra<sup>5,6</sup>. The addition of loudspeaker sources provides  
32 an opportunity for optimizing the acoustic field within a chamber, as will be shown in this  
33 paper. Synthesizing diffuse fields below the Schroeder frequency can lead to significant  
34 financial and time savings. For instance, physical dimensions of new chambers could be  
35 relaxed and shipping of test articles across facilities could be eliminated.

36 The design of diffuse acoustic fields has been explored, to some extent, in the open  
37 literature. Specific examples include the work of Bravo and Maury<sup>7</sup> who designed various  
38 types of acoustic random fields, including diffuse fields, using direct acoustic field testing.  
39 To that end, they solved a quadratic optimization problem in which they found correlated  
40 sources that minimized the misfit between the predicted field and the spatial correlation of  
41 the target random field near the surface of a test body. In recent work, Alvarez-Blanco et  
42 al.<sup>8</sup> presented an approach to design controls for an array of loud speakers to create diffuse  
43 fields in direct acoustic tests. For this, they also used a pseudo-inverse strategy to obtain  
44 solutions of a quadratic optimization problem that directly provided the signal inputs. For  
45 other relevant, recent work in this area see<sup>9-11</sup>.

46 As in the aforementioned work, we are interested in designing diffuse fields. However, in  
47 contrast to the existing literature, we investigate the synthesis of these fields in reverberant  
48 rooms at arbitrary frequencies (even below the Schroeder limit). Hence, our main contribu-  
49 tion is the development of a numerical approach for the design of acoustic diffuse fields in  
50 enclosed rooms. To that end, we put forward a PDE-constrained optimization formulation  
51 for the control problem. Although existing work has addressed the Multiple Input Multiple  
52 Output (MIMO) control problem<sup>7,8</sup>, we provide further insight into Tikhonov regularization

53 for these problems. Moreover, one of the numerical challenges in designing or producing  
54 samples of a diffuse field in simulations is the need to capture its spatial correlation. The  
55 latter may require fine discretizations (e.g. using finite elements) that lead to large dense  
56 matrices.

57 The computational challenge of factorizing the spatial correlation (in the context of diffuse  
58 fields) was recently addressed in<sup>12</sup>, who proposed to generate diffuse fields given by expan-  
59 sions on the eigenfunctions of the pressure correlation operator (i.e. using the Karhunen-  
60 Loève decomposition of the latter). To avoid the computational bottleneck of factorizing a  
61 dense correlation, they employed a low-order Taylor expansion in Cartesian components of  
62 the relative position vector, approximating the continuous correlation function while ensur-  
63 ing the vector does not exceed the operating wavelength significantly. This approximation  
64 reduced the correlation to a product of univariate kernels, whose eigenfunctions are recog-  
65 nized as spheroidal wave functions

66 In contrast, our approach exploits a more-accurate low-rank approximation of the cor-  
67 relation function, applicable to arbitrary sets of target points. This allows us to solve the  
68 least-squares problem producing an optimal design at a computational cost that grows only  
69 linearly with the (potentially large) number of target points (instead of quadratically if us-  
70 ing directly the dense correlation matrix). In addition, this proposed treatment allows us to  
71 formulate simple and efficient regularized versions of the optimization problem, which cater  
72 to it being possibly ill-conditioned and remain computationally economical.

73 The rest of the paper is organized as follows. We provide a summary of the plane-wave  
74 model for diffuse fields and the ensuing statistics. We then formulate the forward problem

75 for modeling a random acoustic field in an enclosed room. Next, we provide the optimization  
76 formulation for the control problem and the description of our approach for the low-rank  
77 approximation of the spatial correlation. We also offer two Tikhonov regularization strategies  
78 for the control problem. Next, we demonstrate the feasibility of our proposed strategy using  
79 numerical examples in an enclosed room driven at frequencies below the Schroeder limit.  
80 Finally, we provide some conclusions and future directions.

## 81 II. BACKGROUND

82 Here we summarize existing results on the theoretical modeling of diffuse fields. We will  
83 adopt the plane wave model in which a random pressure field is conceived as the interaction  
84 of an infinite number of plane waves with randomized direction and phase<sup>13</sup>. It is well  
85 known that this model leads to a Gaussian spatio-temporal pressure field, which is fully  
86 characterized by its mean and correlation function. In this work, for the sake of simplicity  
87 and without loss of generality, we will concentrate on pure-tone fields.

### 88 A. Plane Wave Model

89 Following Jacobsen<sup>14</sup>, we model a pure-tone diffuse field as a random pressure field ex-  
90 pressed as

$$P(\mathbf{x}, \omega; \theta) = \lim_{N \rightarrow \infty} \frac{1}{\sqrt{N}} \sum_{n=1}^N A_n e^{-i(\kappa \mathbf{D}_n \cdot \mathbf{x} + \Phi_n)} \quad (2)$$

91 where  $\kappa = \omega/c$  is the wave number,  $c$  is the speed of sound,  $\mathbf{D}_n$  are independent random  
92 vectors (uniformly distributed over the unit sphere) describing the direction of a plane wave,

93  $A_n$  are independent random variables, and  $\Phi_n$  are random phases. The vector  $\theta$  represents  
 94 the collection of all the random variables in the model. Notice that, as a consequence of  
 95 the Central Limit Theorem, the random field  $P(\mathbf{x}, \omega; \theta)$  is Gaussian<sup>14</sup>. Also, without loss of  
 96 generality, we use in the sequel a constant value  $A_n := p_0$ .

## 97 B. First and Second Order Statistics of a Diffuse Field

98 Here we summarize well-known results on the statistics of the stochastic field shown in  
 99 (2). It is straightforward to show that

$$\mathbb{E}[P(\mathbf{x}, \omega; \theta)] = 0 \quad \forall \mathbf{x}, \omega$$

100 where  $\mathbb{E}[\cdot]$  denotes expectation.

Let  $r_{qs} = \|\mathbf{x}_q - \mathbf{x}_s\|$  be the distance between any two points  $\mathbf{x}_q$  and  $\mathbf{x}_s$ . Then, the correlation can be shown to be given by<sup>15</sup>

$$\begin{aligned} G(r_{qs}, \omega) &= \mathbb{E}[P(\mathbf{x}_q, \omega; \theta)\overline{P(\mathbf{x}_s, \omega; \theta)}] \\ &= \frac{p_0^2}{2} \frac{\sin(\kappa(\omega)r_{qs})}{\kappa(\omega)r_{qs}} \end{aligned} \quad (3)$$

101 where the overbar denotes complex conjugation.

102 As previously noted, the random field  $P(\mathbf{x}, \omega; \theta)$  is Gaussian. Hence, we can completely  
 103 characterize the diffuse field through its mean and correlation. Moreover, the field is weakly  
 104 isotropic (i.e. the mean is constant and the correlation depends only on the distance between  
 105 two points)<sup>16</sup>. A more extensive discussion on diffuse fields can be found in<sup>14,15,17,18</sup>.

106 **III. DESIGN OF DIFFUSE FIELDS**

107 As stated before, we seek to develop a numerical framework for designing approximately  
 108 diffuse fields for rooms of any shape and size at arbitrary frequencies. To this end, we  
 109 first introduce the acoustic equations and numerical approximations, followed by the design  
 110 problem, and a formal regularized treatment of the ensuing ill-posed design problem.

111 As we will see later in this section, one of the key challenges in the design problem is the  
 112 computational expense that arises from the discretization of the target correlation function.  
 113 One of our contributions in this work is an efficient low-rank representation of the target  
 114 correlation that renders the design problem tractable.

115 **A. Forward Problem**

We model a room as a bounded domain  $\Omega \subset \mathbb{R}^3$  with boundary (walls)  $\Gamma$ . The part of  
 the walls with impedance conditions is denoted as  $\Gamma_r$ , while that occupied by the speakers  
 is denoted as  $\Gamma_N = \cup_j \Gamma_{N_j}, j = 1 \dots d$ , where  $d$  is the number of speakers in the room and  
 $\Gamma = \Gamma_r \cup \Gamma_N$ . The pressure field in the room satisfies<sup>19</sup>

$$\begin{aligned} \nabla^2 p + \kappa^2 p &= 0 \quad \text{in } \Omega \\ \nabla p \cdot \mathbf{n} + iZ^{-1}\omega\rho_0 p &= 0 \quad \text{on } \Gamma_r \\ \nabla p \cdot \mathbf{n}_j - \rho_0 s_j &= 0 \quad \text{on } \Gamma_{N_j} \quad \text{for } j = 1, \dots, d \end{aligned} \tag{4}$$

116 where  $\omega$  is the angular frequency,  $\rho_0$  is the fluid density,  $\kappa$  is the wavenumber,  $s_j$  is the  
 117 normal acoustic acceleration over  $\Gamma_j$ ,  $Z$  is the specific acoustic impedance, and  $\mathbf{n}_j$  is a unit  
 118 vector normal to  $\Gamma_j$  and directed out of the room. Using the Finite Element Method<sup>20</sup> to

119 obtain a discrete representation of (4), we arrive at

$$R\mathbf{p} = F\mathbf{s}$$

120 where  $R := K - \kappa^2 M + i\omega C$ ,  $K$  is the acoustic stiffness,  $M$  is the mathematical mass matrix,  
 121  $C$  is the damping matrix,  $F \in \mathbb{R}^{N \times d}$  is a matrix that acts on the acoustic accelerations vector  
 122  $\mathbf{s} \in \mathbb{R}^d$ .

Let  $\mathcal{T} := \{\mathbf{x}_1, \dots, \mathbf{x}_m\}$  be a finite set of  $m$  target locations where we want the field to be diffuse. Now, let  $B \in \mathbb{R}^{m \times d}$  be the Boolean matrix such that  $\mathbf{p}_{\mathcal{T}} = B\mathbf{p} \in \mathbb{C}^m$  collects the nodal pressures at the target locations. We then have

$$\begin{aligned} \mathbf{p}_{\mathcal{T}} &= B\mathbf{p} \\ &= BR^{-1}F\mathbf{s} \\ &= T\mathbf{s} \end{aligned}$$

123 where we have introduced the transfer matrix  $T := BR^{-1}F \in \mathbb{C}^{m \times d}$ . Also, we point out that  
 124 if  $Z \neq 0$ ,  $R$  is invertible for any frequency<sup>21</sup>.

For random sources, the relationship between the cross-correlation of the target pressures denoted as  $G$ , and the cross-correlation of the sources, denoted as  $S$ , at a given frequency is given as

$$\begin{aligned} G &= \mathbb{E}[\mathbf{p}_{\mathcal{T}}\mathbf{p}_{\mathcal{T}}^h] \\ &= T \mathbb{E}[\mathbf{s}\mathbf{s}^h] T^h \\ &= TST^h \end{aligned} \tag{5}$$



125 where the superscript  $h$  denotes complex conjugation and transposition. So, given  $S$ , we  
 126 can compute  $G$  at given locations. Next, we develop a design methodology for diffuse fields  
 127 based on the forward model presented in this section.

## 128 **B. Inverse or Design Problem**

129 Our design problem can be described as: given a cross-correlation at a set  $\mathcal{T}$  of target  
 130 nodes, determine the cross-correlation of the input sources. To this end, let  $\mathbf{x}_i, \mathbf{x}_j \in \mathcal{T}$  be  
 131 two target locations. Then, from (3), the components of the target cross-correlation matrix  
 132 at a given frequency,  $\hat{G}_{ij}$ , are given as

$$\hat{G}_{ij} = \frac{p_o^2 \sin(\kappa r_{ij})}{2 \kappa r_{ij}} \quad (6)$$

133 We first introduce an un-regularized inverse problem for the sake of simplicity. This  
 134 formulation leads to a decomposition of the inverse problem that strongly reduces compu-  
 135 tational cost, as will be shown. After this, a regularized version of the problem follows  
 136 naturally. Define an objective function as

$$J(S) := \frac{1}{2} \|G(S) - \hat{G}\|_F^2 \quad (7)$$

137 where  $G(S)$  solves (5) and  $\|G\|_F$  is the Frobenius matrix norm, which is associated with an  
 138 inner product:  $\|G\|_F^2 = (G, G)_F =: \text{tr}(G^h G)$ . Then, the optimal cross-correlation,  $S_o$ , can  
 139 be obtained as

$$S_o = \arg \min_{S \in \mathbb{C}^{d \times d}} J(S). \quad (8)$$

140 While the search space for the above minimization should *a priori* be restricted to positive  
 141 definite and Hermitian matrices  $S$ , it turns out that the minimum-norm solution found by  
 142 the unconstrained minimization (8) automatically satisfies those requirements, see Remark 3.

### 143 C. Optimality Condition and minimum-norm least-squares solution

144 To simplify our derivations, define a linear operator  $\mathcal{A} : \mathbb{C}^{d \times d} \rightarrow \mathbb{C}^{m \times m}$  as

$$\mathcal{A}S := TST^h \tag{9}$$

145 Substituting this expression into the objective (7), we get

$$J(S) := \frac{1}{2} \|\mathcal{A}S - \hat{G}\|_F^2$$

The first-order optimality condition for Problem (8) is that the gradient of the objective be zero at the minimizer. Using the inner product associated with the Frobenius norm, the directional derivative of the objective at  $S \in \mathbb{C}^{d \times d}$  in an arbitrary direction  $H \in \mathbb{C}^{d \times d}$  is obtained as

$$\begin{aligned} \langle J'(S), H \rangle &= \left. \frac{d}{d\epsilon} J(S + \epsilon H) \right|_{\epsilon=0} \\ &= \operatorname{Re}(\mathcal{A}S - \hat{G}, \mathcal{A}H)_F \\ &= \operatorname{Re}(\mathcal{A}^* \mathcal{A}S - \mathcal{A}^* \hat{G}, H)_F \end{aligned}$$

146 where  $\mathcal{A}^*$  denotes the adjoint of  $\mathcal{A}$ , defined by  $(W, \mathcal{A}V)_F = (\mathcal{A}^*W, V)_F$  for any  $W \in \mathbb{C}^{m \times m}$   
 147 and  $V \in \mathbb{C}^{d \times d}$ . Then, from the above expression, the first-order optimality condition  
 148  $J'(S_o) = 0$  verified by  $S_o$  is obtained as

$$\mathcal{A}^* \mathcal{A}S_o - \mathcal{A}^* \hat{G} = 0, \tag{10}$$

149 which is in essence the normal equation for the least squares problem (8). Then, using (9)  
 150 in (10) and simplifying, we get

$$T^h T S_o T^h T = T^h \hat{G} T$$

151 If  $T^h T$  is not invertible (i.e. if  $T$  does not have full column rank  $d$ ), the above equation fails  
 152 to provide a solution  $S_o \in \mathbb{C}^{d \times d}$  that is invertible (let alone positive definite). The transfer  
 153 matrix  $T$  is therefore assumed henceforth to have rank  $d$ .

154 To solve equations (10), and also to later address regularized versions of Problem (8), it  
 155 is convenient and computationally reasonable (under the present operating conditions) to  
 156 introduce and use the reduced singular value decomposition (SVD) of  $T$ :

$$T = X \Sigma Y^h, \tag{11}$$

157 where  $\Sigma \in \mathbb{R}^{d \times d}$  is a diagonal matrix holding the  $d$  nonzero singular values  $\sigma_1 \geq \sigma_2 \geq$   
 158  $\dots \sigma_d > 0$  of  $T$  while  $X \in \mathbb{C}^{m \times d}$  and  $Y \in \mathbb{C}^{d \times d}$  hold the  $d$  left and right associated singular  
 159 vectors (arranged columnwise), respectively. In particular, the matrices  $X$  and  $Y$  have the  
 160 orthonormality properties  $X^h X = I_d$  and  $Y^h Y = Y Y^h = I_d$ , with  $I_d$  the  $d \times d$  identity  
 161 matrix. On introducing the SVD (11) in (10) and using the latter properties of  $X$  and  $Y$ ,  
 162 the minimum-norm least-squares solution  $S_o$  is found as

$$S_o = Y \Sigma^{-1} (X^h \hat{G} X) \Sigma^{-1} Y^h. \tag{12}$$

163 and is clearly Hermitian and positive definite. Moreover, for any  $\mathbf{s} \in \mathbb{C}^d$ , we have  $\mathbf{s}^h S_o \mathbf{s} =$   
 164  $(X \Sigma^{-1} Y^h \mathbf{s})^h \hat{G} (X \Sigma^{-1} Y^h \mathbf{s}) > 0$  by virtue of the positive definiteness of  $\hat{G}$ , showing that  $S_o$   
 165 is in fact positive definite.

166 The expression (12) of  $S_o$  entails the evaluation of  $X^h \hat{G} X$ , whose  $O(dm^2 + d^2m/2)$  cost  
 167 constitutes a potential computational bottleneck as  $\hat{G}$  is a dense  $m \times m$  matrix that may  
 168 be large in realistic problems (e.g.  $m = O(10^4)$  to  $O(10^6)$ ). To reduce the computational  
 169 complexity in  $m$  of the design solution method, we now introduce a low-rank approximation  
 170 of  $\hat{G}$ .

#### 171 D. Low-rank approximation of $\hat{G}$

172 The target correlation  $\hat{G}$  being symmetric and positive definite, we have  $\hat{G} = \sum_{k=1}^m \psi_k \psi_k^h \lambda_k$ ,  
 173 where  $\psi_k, \lambda_k$  are the eigenpairs of  $\hat{G}$  numbered so that  $\lambda_1 \geq \lambda_2 \dots \geq \lambda_m > 0$ . By the Eckart-  
 174 Young theorem, this expansion, truncated to its first  $P$  terms, yields the best rank- $P$   
 175 approximation of  $\hat{G}$ , denoted as  $\hat{G}_P$ , in the sense of the Frobenius norm. Specifically, the  
 176 relative truncation error is given as

$$\mathcal{E}^2(P) := \frac{\|\hat{G} - \hat{G}_P\|_F^2}{\|\hat{G}\|_F^2} = \frac{\sum_{k=P+1}^m \lambda_k^2}{\sum_{j=1}^m \lambda_j^2} \quad (13)$$

177 The rate of decay of the eigenvalues of a correlation matrix depends on the correlation  
 178 length. The latter is usually high, which allows a truncation order  $Q \ll m$ . However, setting  
 179 up this approximation still entails obtaining a large enough number of eigenpairs of the  
 180  $m \times m$  matrix  $\hat{G}$  to achieve and verify a sufficiently low truncation error, and this remains  
 181 often impractical.

182 We therefore propose an alternative strategy for deriving low-rank approximations of  $\hat{G}$ .  
 183 It is based on observing that the generic entry  $\hat{G}_{ij}$  of  $\hat{G}$ , see (6), is in fact equivalently given

$$\hat{G}_{ij} = \frac{p_o^2}{2} j_0(\kappa |\mathbf{r}_{ij}|)$$

185 where  $j_0$  is the spherical Bessel function of first kind and order zero and  $\mathbf{r}_{ij} := \mathbf{x}_i - \mathbf{x}_j$  is  
 186 the position vector joining two generic target points. Now, for any  $\mathbf{z} \in \mathbb{R}^3$ , the function  $j_0$   
 187 admits the integral representation

$$j_0(|\mathbf{z}|) = \frac{1}{4\pi} \int_{\hat{S}} e^{i\mathbf{z} \cdot \hat{\boldsymbol{\theta}}} dS(\hat{\boldsymbol{\theta}}), \quad (14)$$

188 where  $\hat{S}$  is the unit sphere (spanned by unit vectors  $\hat{\boldsymbol{\theta}}$ ). For instance, expressing the above  
 189 integral using spherical angular coordinates reduces it to the one-dimensional integral repre-  
 190 sentation formula (10.54.1) given in<sup>22</sup>. Let the above integral be approximated by a  $Q$ -point  
 191 quadrature rule with nodes  $\hat{\boldsymbol{\theta}}_q \in \hat{S}$  and positive weights  $w_q$  ( $1 \leq q \leq Q$ ), yielding

$$j_0(|\mathbf{z}|) = \left( \frac{1}{4\pi} \sum_{q=1}^Q w_q e^{i\mathbf{z} \cdot \hat{\boldsymbol{\theta}}_q} \right) + \varepsilon_Q,$$

192  $\varepsilon_Q$  being the quadrature error. Setting  $\mathbf{z} = \kappa(\mathbf{x}_i - \mathbf{x}_j)$ , we thus approximate  $\hat{G}_{ij}$  as

$$\hat{G}_{ij} \approx \frac{p_o^2}{8\pi} \sum_{q=1}^Q w_q e^{i\mathbf{x}_i \cdot \hat{\boldsymbol{\theta}}_q} e^{-i\mathbf{x}_j \cdot \hat{\boldsymbol{\theta}}_q},$$

193 a result which in turn yields, upon application to all pairs of target points, the following  
 194 (approximate) decomposition of the target correlation matrix  $\hat{G}$ :

$$\hat{G} \approx \Phi \Phi^h = \sum_{q=1}^Q \boldsymbol{\phi}_q \boldsymbol{\phi}_q^h, \quad \Phi = [\boldsymbol{\phi}_1, \dots, \boldsymbol{\phi}_Q] \in \mathbb{C}^{m \times Q}, \quad \Phi_{jq} = (\boldsymbol{\phi}_q)_j = \sqrt{w_q} e^{i\mathbf{x}_j \cdot \hat{\boldsymbol{\theta}}_q}. \quad (15)$$

195 The size  $Q$  of the quadrature rule ensuring a desired (small enough) quadrature error depends  
 196 on the oscillatory character of the integral (14), and hence on the magnitude of the argument  
 197  $|\mathbf{z}|$  of  $j_0$  there. In this study, the latter is bounded from above by the largest spatial

198 separation between target points and the operating frequency. Consequently,  $Q$  does not  
 199 depend on the number  $m$  of target points once their maximum spatial separation is fixed.  
 200 In the forthcoming examples,  $Q = O(10^2)$  whereas  $m = O(10^4)$ , so that (15) accomplishes a  
 201 low-rank approximation of  $\hat{G}$ , whose computation is moreover economical as the  $m$ -vectors  
 202  $\phi_q$  are given explicitly.

203 The low-rank approximation (15) greatly reduces the computational load in evaluating  
 204  $S_o$ . Indeed, using (15) in (12) gives

$$S_o = (Y\Sigma^{-1}Z)(Y\Sigma^{-1}Z)^h, \quad Z := X^h\Phi \in \mathbb{C}^{d \times Q},$$

205 whose evaluation needs only  $O(m)$  computational work and memory, down from  $O(m^2)$  if  
 206 using the full matrix  $\hat{G}$ .

207 **Remark 1** *Unlike in the expansion  $\hat{G} = \sum_{q=1}^m \psi_q \psi_q^T \lambda_q$  in terms of eigenpairs, the vectors*  
 208  *$\phi_q$  in (15) are not orthogonal.*

## 209 E. Regularized least-squares solution

210 We now address the case where  $T^h T$  may be ill-conditioned (i.e. have a large condition  
 211 number), with  $T$  still assumed to have full column rank. Let

$$\mathbf{s}_q = Y\Sigma^{-1}X^h\phi_q \tag{16}$$

212 Then, the minimum-norm solution to (8) is given by

$$S_o = \sum_{q=1}^Q \mathbf{s}_q \mathbf{s}_q^h \tag{17}$$

213 We notice that  $\mathbf{s}_q$  given by (16) is (by our assumption on  $T$ ) the unique solution of the  
 214 least-squares problem

$$\mathbf{s}_q = \arg \min_{\mathbf{u} \in \mathbb{C}^d} \frac{1}{2} \|T\mathbf{u} - \phi_q\|_2^2 \quad (18)$$

215 where  $\|\cdot\|_2$  is the Euclidean norm. Therefore, to obtain  $S_o$  given by (17), we have to solve  
 216 at most  $Q$  problems of the type (18). To cater for  $T^h T$  being possibly ill-conditioned, we  
 217 add a regularization term in (18) to get the problem

$$\mathbf{s}_q(\alpha) = \arg \min_{\mathbf{u} \in \mathbb{C}^d} \frac{1}{2} \left( \|T\mathbf{u} - \phi_q\|_2^2 + \alpha \|\mathbf{u}\|_2^2 \right), \quad (19)$$

218 (where  $\alpha > 0$  is a regularization parameter), whose unique minimizer is given in closed form  
 219 as

$$\mathbf{s}_q(\alpha) = Y(\Sigma + \alpha I)^{-1} X^h \phi_q. \quad (20)$$

220 The resulting input correlation matrix is then given by

$$S_{o1}(\alpha) := \sum_{q=1}^Q \mathbf{s}_q(\alpha) \mathbf{s}_q^h(\alpha) = (Y(\Sigma + \alpha I)^{-1} Z) (Y(\Sigma + \alpha I)^{-1} Z)^h. \quad (21)$$

We can show that  $S_{o1}(\alpha)$  converges to the minimum-norm solution  $S_{o1}$  of our original problem (8) as  $\alpha \rightarrow 0$ . Indeed, from (16) and (20), we have

$$\begin{aligned} \mathbf{s}_q(\alpha) - \mathbf{s}_q &= Y[(\Sigma + \alpha I)^{-1} - \Sigma^{-1}] X^h \phi_q \\ &= Y(\Sigma + \alpha I)^{-1} [I - (\Sigma + \alpha I)\Sigma^{-1}] X^h \phi_q \\ &= -\alpha Y(\Sigma + \alpha I)^{-1} \Sigma^{-1} X^h \phi_q \end{aligned}$$

221 Therefore,  $\|\mathbf{s}_q(\alpha) - \mathbf{s}_q\| \rightarrow 0$  and  $\|S_{o1}(\alpha) - S_o\|_F \rightarrow 0$  as  $\alpha \rightarrow 0$  (since  $S_{o1}(\alpha)$  and  $S_o$  are  
 222 both given by finite sums of tensor products)

223 *Second regularization method*

224 Alternatively, we can consider the regularized version

$$S_{o2}(\alpha) := \arg \min_{S \in \mathbb{C}^{d \times d}} J_\alpha(S), \quad J_\alpha(S) := \frac{1}{2} \|\mathcal{A}S - \hat{G}\|_F^2 + \frac{\alpha}{2} \|S\|_F^2 \quad (22)$$

225 of the original least-squares problem (8), whose stationarity condition is

$$T^h T S_{o2}(\alpha) T^h T + \alpha S_{o2}(\alpha) = T \hat{G} T^h.$$

226 Invoking again the reduced SVD (11) of  $T$ , the above equation becomes

$$\Sigma^2 H(\alpha) \Sigma^2 + \alpha H(\alpha) = \Sigma \hat{H} \Sigma, \quad \text{with } H := Y^h S_{o2}(\alpha) Y. \quad (23)$$

227 Since  $\Sigma$  is diagonal, the above equation decouples into componentwise scalar equations

228 whereby

$$H_{ij}(\alpha) = \frac{\sigma_i \sigma_j}{\sigma_i^2 \sigma_j^2 + \alpha} (Z Z^h)_{ij} \quad 1 \leq i, j \leq d, \quad (24)$$

229 and  $S_{o2}(\alpha) = Y H(\alpha) Y^h$  is readily found once  $H(\alpha)$  is evaluated using the above formula.

230 Moreover, it is easy to verify that (24) with  $\alpha = 0$  yields  $S_o = Y H(0) Y^h$  through (12), and

231 that we have

$$H_{ij}(\alpha) - H_{ij}(0) = -\frac{\alpha}{\sigma_i \sigma_j (\sigma_i^2 \sigma_j^2 + \alpha)} (Z Z^h)_{ij} \quad 1 \leq i, j \leq d.$$

232 Consequently, this second regularization approach also verifies  $\|S_{o2}(\alpha) - S_o\| \rightarrow 0$  as  $\alpha \rightarrow 0$ .

233 **Remark 2** *The first regularization yields  $H_{ij}(\alpha) = (Z Z^h)_{ij} / (\sigma_i + \alpha)(\sigma_j + \alpha)$  instead of (24),*

234 *with  $H_{ij}$  as in (23). This shows that the two regularization approaches are not identical,*

235 *although the next remarks 3, 4 show that they are similar in several ways.*



236 **Remark 3** *The minimum-norm solution  $S_o$  to problem (8), as well as its regularized ap-*  
237 *proximations  $S_{o1}(\alpha)$  and  $S_{o2}(\alpha)$ , are Hermitian and positive definite (and hence acceptable*  
238 *as correlation matrices), without those restrictions needing to be explicitly enforced (e.g.*  
239 *through constraints). In fact, any matrix  $S \in \mathbb{C}^{d \times d}$  can be additively decomposed into its*  
240 *Hermitian and skew-Hermitian parts:  $S = S_1 + S_2$  with  $S_1^h = S_1$  and  $S_2^h = -S_2$ , and we have*  
241  *$\|S\|_F^2 = \|S_1\|_F^2 + \|S_2\|_F^2$ . Moreover, it is easy to verify that  $G_1 := \mathcal{A}(S_1)$  and  $G_2 := \mathcal{A}(S_2)$*   
242 *are respectively Hermitian and skew-Hermitian. For the objective functional  $J(S)$ , this gives*  
243 *(since  $\hat{G}$  is Hermitian)*

$$2J(S) = \|G_1 - \hat{G}\|_F^2 + \|G_2\|_F^2,$$

244 *so that optimality implies  $G_2 = 0$ , hence  $S_2 = 0$  since by assumption  $T$  has full (column)*  
245 *rank. A similar line of reasoning applies to the regularized versions of problem (8).*

246 **Remark 4** *From a computational complexity standpoint, both regularizations require  $O(md^2) +$*   
247  *$O(Qd^2) + O(d^3)$  complex arithmetic operations, with  $m \gg Q \geq d$  in the present context. The*  
248 *leading  $C \times md^2$  amount of arithmetic operations (where  $C$  is a method-dependent constant)*  
249 *arises from the decomposition of the transfer matrix  $T$ . Both regularization methods may (as*  
250 *explained) use the reduced SVD of  $T$ , in which case  $C = 6^{23}$  (Sec. 8.6). Alternatively, the*  
251 *first regularization may as easily be carried out using a thin QR factorization of  $[T; \sqrt{\alpha}I]$ ,*  
252 *resulting in  $C = 2^{23}$  (Sec. 5.2).*

## 253 IV. NUMERICAL RESULTS

### 254 A. Problem Description

255 In this section, we demonstrate how we can construct approximate diffuse fields in en-  
256 closed rooms for arbitrary frequencies (e.g. below the Schroeder frequency). That is, by  
257 driving the room with signals drawn from a multivariate Gaussian vector with zero mean  
258 and an optimal speaker correlation, we can obtain a random field in the target region whose  
259 spatial cross-correlation is close to (3) in the sense described by (8).

260 We consider a room with dimensions  $5.75 \times 4.25 \times 3 \text{ m}^3$ . The impedance for the wall,  
261 roof, and floor is taken constant for all simulations and set to  $Z = 4.25 \times 10^5 \text{ kg}/(\text{m}^2 \text{ s})$ ,  
262 while the speed of sound and mass density are  $c = 340 \text{ m/s}$  and  $\rho_0 = 1 \text{ kg}/\text{m}^3$ . The side  
263 walls of the room contain uniformly spaced speakers each with an area of  $0.25 \times 0.25 \text{ m}^2$ . We  
264 consider three different speaker configurations in this study: 1) 9 speakers/wall ( $d = 36$ ), 2)  
265 16 speakers/wall ( $d = 64$ ), and 3) 25 speakers/wall ( $d = 100$ ). For each case, we compute  
266 optimal speaker correlations for three frequencies: 150, 250, and 300 Hz. A representative  
267 geometry for the room with 36 speakers is shown in Figure 1. The target region, also shown,  
268 has dimensions  $2 \times 2 \times 2 \text{ m}^3$  and is located in the center of the room.

269 For each of the studied cases, we first compute a low-rank approximation of the target  
270 correlation  $\hat{G}$  as per (15), using  $Q = 200$ . This quadrature rule results in a relative ap-  
271 proximation error of less than 0.1% on  $\hat{G}$  for all cases studied herein. We then solve the  
272 least-squares problems (19) for  $1 \leq q \leq Q$ . Finally, the optimal speaker cross-correlation  $S_o$   
273 is obtained as per (21). The Tikhonov regularization parameter  $\alpha$  is determined using an

274 L-curve approach<sup>24,25</sup>. To this end, we use the objective and regularization term in (22) for  
 275 either of the regularization strategies described in Section III E. We point out that the com-  
 276 putational cost of solving all the aforementioned optimization problems is negligible when  
 277 compared to the computational cost of building the transfer matrix  $T$ .

278 We use an in-house Finite Element code developed using the FEniCS library<sup>26</sup> in conjunc-  
 279 tion with the parallel direct solver MUMPS for all the calculations presented herein. The  
 280 models are meshed with four-node tetrahedral elements. All the results shown are generated  
 281 with a mesh containing approximately 130,000 nodes and 750,000 elements, which is fine  
 282 enough to achieve a low discretization error in all calculations.

283 The Schroeder frequency for this room is calculated from (1). The reverberation time is  
 284 estimated using the Norris-Eyring relation<sup>27</sup>:

$$T_{60} = \frac{-24V \ln(10)}{A c \ln(1 - \alpha_{rand})},$$

285 where  $A = 2(L_x L_y + L_x L_z + L_y L_z)$  is the room surface area and  $\alpha_{rand}$  the random-incidence  
 286 absorption coefficient<sup>19</sup>

$$\alpha_{rand} = 1 - \int_0^{\pi/2} \left| \frac{Z \cos(\theta) - \rho_0 c}{Z \cos(\theta) + \rho_0 c} \right|^2 \sin(2\theta) d\theta.$$

287 Using the above expressions in (1), we obtain  $f_s = 1001$  Hz. Hence, we point out the  
 288 frequencies used in the examples (150, 250, and 300 Hz) are well below the Schroeder limit  
 289 for this room.

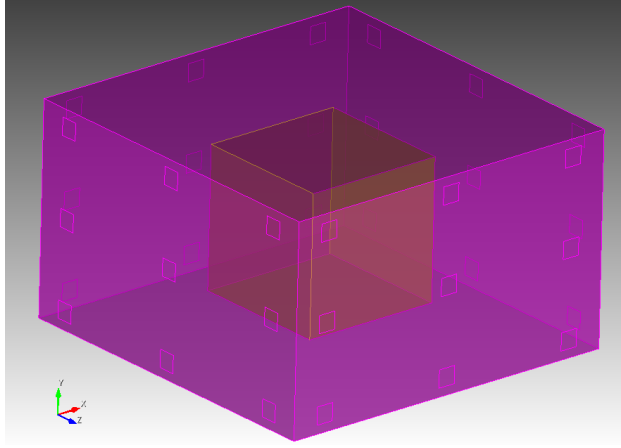


FIG. 1. Room Geometry

290 **B. Results**

291 Let's first define the relative error in correlation (or residual) as

$$\epsilon_G := \frac{\|\mathcal{A}S_o - \hat{G}\|_F}{\|\hat{G}\|_F}$$

292 Without loss of generality, we use  $\frac{p_o^2}{2} = 1$  in all the examples. Hence, a useful metric to  
 293 explore is how much the diagonal entries of  $G^o = \mathcal{A}S_o$  depart from unity. To this end, we  
 294 define the error

$$\epsilon_{ms} := \frac{\sqrt{\sum_i |G_{ii}^o - 1|^2}}{m}$$

295 An equivalent interpretation of this error is how much the mean square pressure (nor-  
 296 malized to unity in our case) departs from being spatially constant. This is a widely used  
 297 metric to judge the level of sound diffusion in laboratory experiments<sup>14,15,17</sup> and proved to  
 298 be very useful for assessing the quality of our numerical solutions.

299 Table I contains a summary of the results along with the Tikhonov parameter ( $\alpha$ ) used in  
 300 each case. We notice that for all frequencies both errors,  $\epsilon_G$  and  $\epsilon_{ms}$ , decrease as the number

TABLE I. Results Summary

	150 Hz			250 Hz			300 Hz		
Speakers	$\epsilon_{ms}$	$\epsilon_G$	$\alpha$	$\epsilon_{ms}$	$\epsilon_G$	$\alpha$	$\epsilon_{ms}$	$\epsilon_G$	$\alpha$
36	0.17	0.33	$2 \times 10^{-3}$	0.35	0.51	$1 \times 10^{-2}$	0.43	0.64	$2 \times 10^{-3}$
64	0.09	0.17	$1 \times 10^{-3}$	0.16	0.30	$1 \times 10^{-2}$	0.18	0.37	$2 \times 10^{-3}$
100	0.08	0.16	$5 \times 10^{-4}$	0.08	0.23	$1 \times 10^{-3}$	0.08	0.24	$5 \times 10^{-4}$

301 of speakers increases, as expected. Another noticeable trend is that these errors increase as  
 302 frequency increases.

303 The increasing trend in approximation errors can be explained by studying how the  
 304 eigenvalues of the target correlation decay as functions of frequency. First, notice that  
 305 the rank of the approximate correlation,  $G_o = TS_oT^h$ , is at most  $d$  (number of speakers).  
 306 Hence, using the best approximation error in Eq. (13), we obtain a lower bound for the  
 307 relative residual of our inverse problem as

$$\frac{\|G_o(d) - \hat{G}\|_F}{\|\hat{G}\|_F} \geq \mathcal{E}(d) \equiv \sqrt{\frac{\sum_{k=d+1}^m \lambda_k^2}{\sum_{j=1}^m \lambda_j^2}} \quad (25)$$

308 Hence, we see that the lower bound depends on the decay of the eigenvalue spectrum. To  
 309 illustrate this behavior in our problem, define a participation factor as

$$P_f^2(d) \equiv \frac{\sum_{k=1}^d \lambda_k^2}{\sum_{j=1}^m \lambda_j^2}$$

310 and notice that  $\mathcal{E}(d)^2 = 1 - P_f^2(d)$ . Now, observe in Fig. 2 how  $P_f(d)$  increases with  
 311 decreasing frequency, in general. The latter trend indicates that the lower bound in Eq. (25)

312 increases with increasing frequency for a fixed truncation level, which is in agreement with  
 313 the error trend reported in Table I.

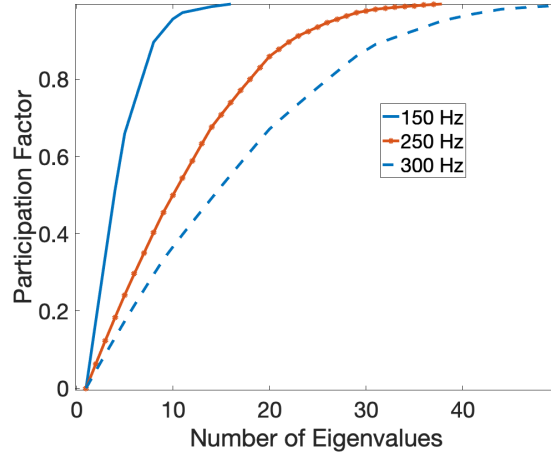


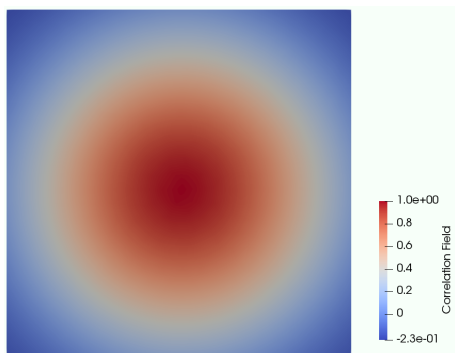
FIG. 2. Participation factor of eigenpairs of the correlation matrix at different frequencies

314

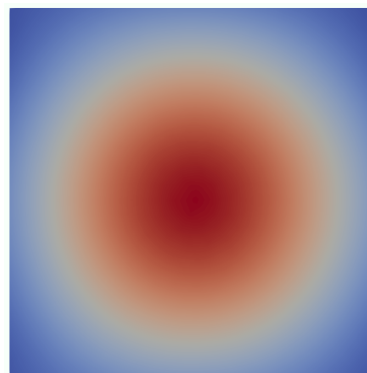
315

316 To better illustrate the quality of our solutions, we plot the correlation field with respect  
 317 to the center of the target region for different combinations of speakers and frequencies as  
 318 shown in Figure 3. We can observe that the optimized correlation closely resembles that of  
 319 a diffuse field. Furthermore, we compare the target and estimated fields along a diagonal  
 320 across the target region in Figure 4. We can again observe a close match of the computed and  
 321 target correlations for different frequency and speaker combinations. It is important to point  
 322 out that we are showing only the target region at the center of the room in these images.  
 323 As we will show later, the acoustic field departs from being purely diffuse at locations near  
 324 the walls, as expected.

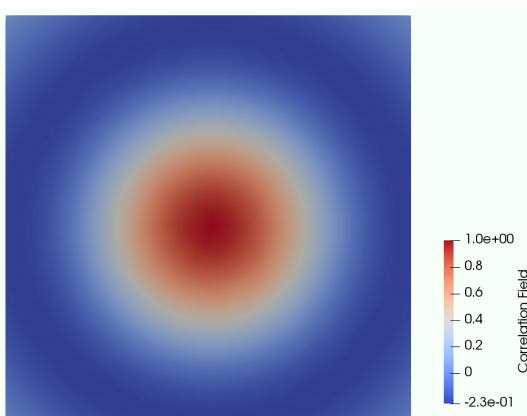
326 Recall that the mean square pressure (i.e. diagonal entries of the correlation) is spatially  
 327 constant in a diffuse field (as captured by the metric  $\epsilon_{ms}$  shown in Table I). We now provide



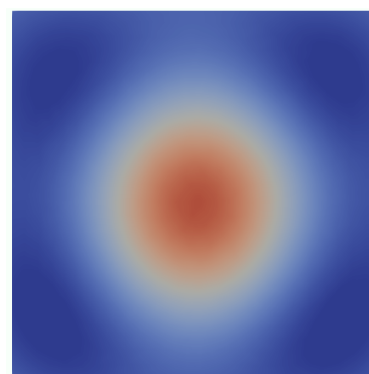
Sinc Function: 150 Hz



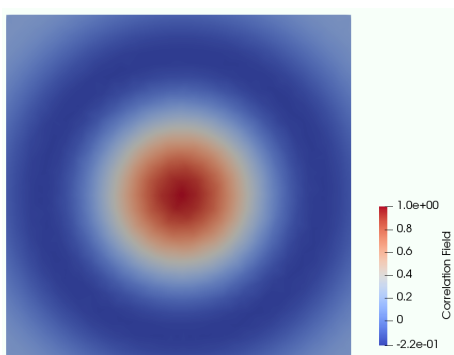
Optimal solution: 150 Hz, 36 speakers



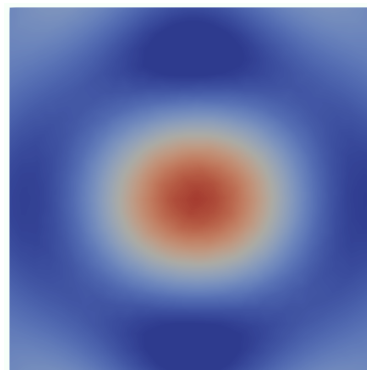
Sinc Function: 250 Hz



Optimal solution: 250 Hz, 64 speakers



Sinc Function: 300 Hz]



Optimal Solution: 300 Hz, 100 speakers

FIG. 3. Correlation field with respect to the center of the target region.

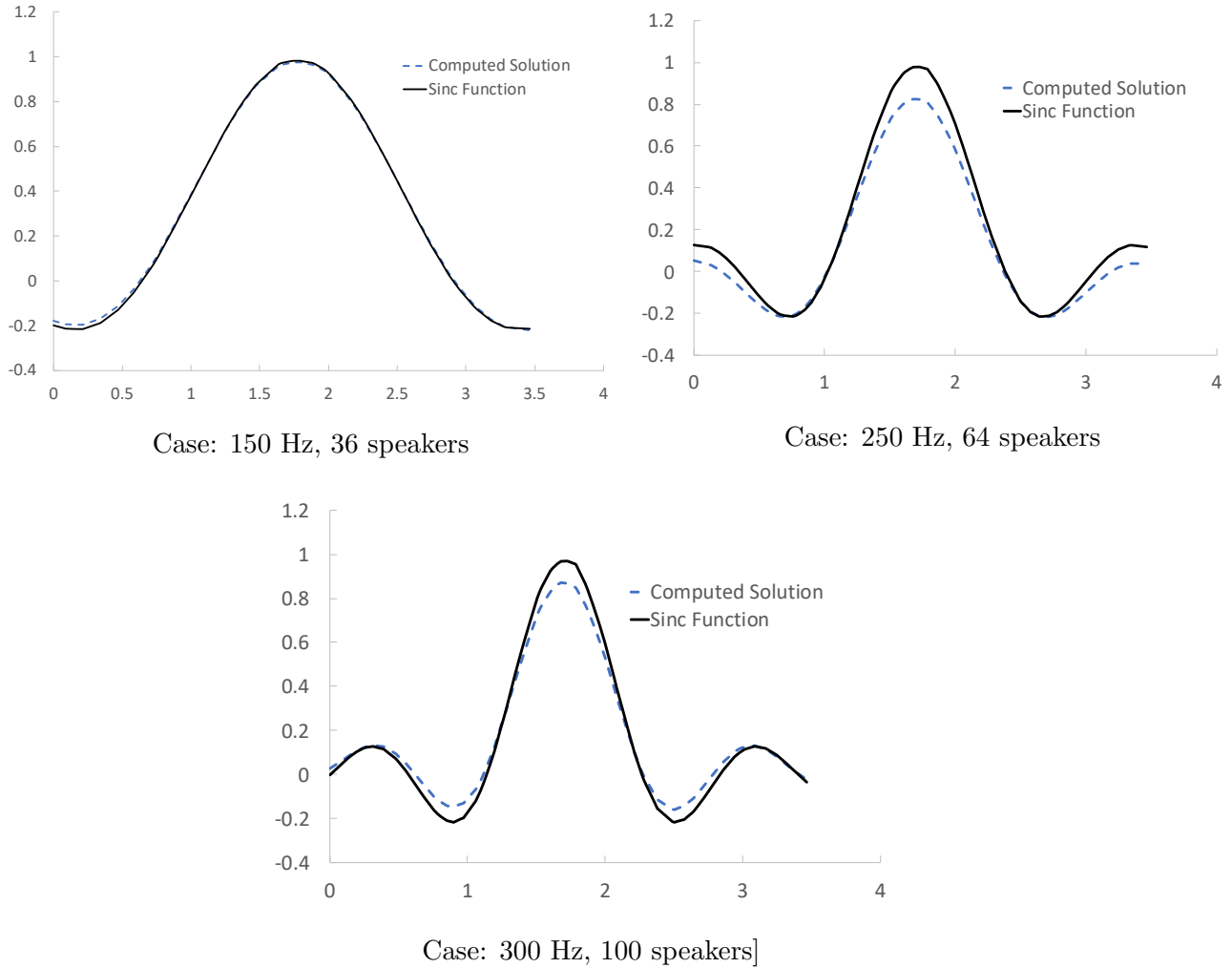


FIG. 4. Correlation field along a diagonal across the target region.

328 more global representations of this behavior. Figure 5(a) shows the mean square pressure  
 329 along a line through the center of the room in the X direction for all cases. We can see that  
 330 the field is close to unity and constant in a region slightly larger than the target domain  
 331 and departs from pure diffusion close to the walls. Furthermore, for comparison purposes,  
 332 we show in Figure 5(b) the mean square pressure obtained using random realizations from  
 333 uncorrelated speakers assuming a standard normal Gaussian distribution. Notice that indeed



334 uncorrelated speakers cannot produce the desired constant field at this given frequency,  
 335 reinforcing the success of the proposed optimization approach.

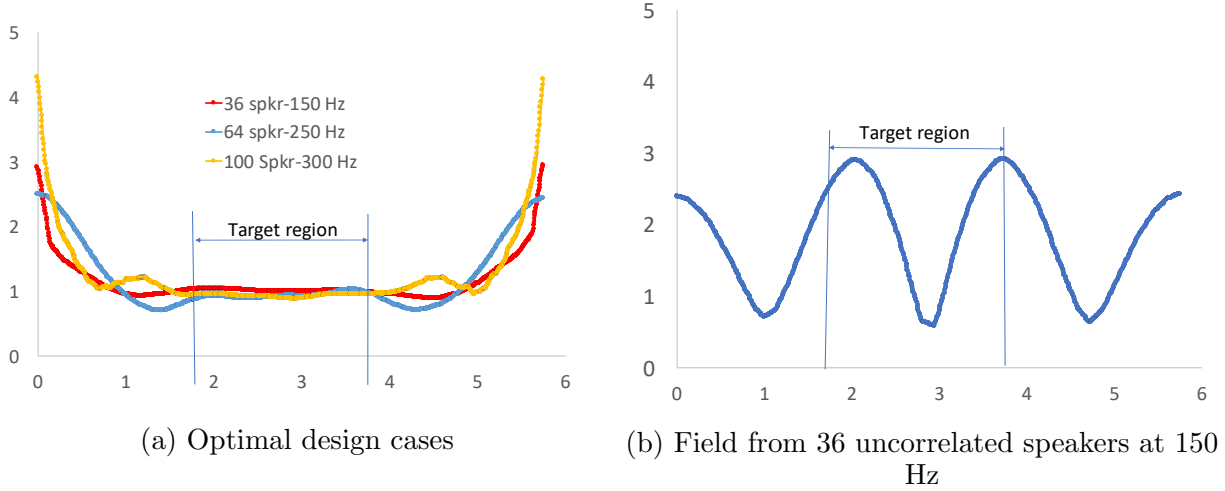


FIG. 5. Mean square pressure in the entire room along X-axis. Results are normalized to be on the same scale as the optimal case.

336 Lastly, Figure 6 shows the mean square pressure field for the three studied cases. Again,  
 337 we notice that, in all cases, the field is constant over a region larger than the target one, but  
 338 departs from diffuse behavior away from the target region, as expected.

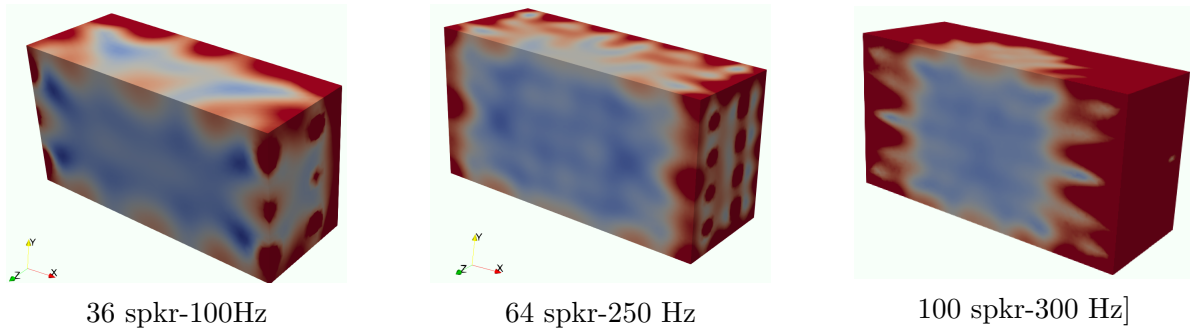


FIG. 6. Mean square pressure in the entire room.

339

340

## 341 V. SUMMARY AND CONCLUSIONS

342 We presented how an optimization approach can be used to produce diffuse fields in  
343 enclosed rooms at arbitrary frequencies (even below the Schroeder limit). To this end, we  
344 characterized a diffuse field solely by its mean and correlation as these are stochastic ho-  
345 mogeneous and isotropic Gaussian processes. Then, we postulated an optimization problem  
346 in which we sought the correlation structure of input speakers that minimized the distance  
347 between the output correlation and that of a diffuse field over a target region. We addressed  
348 the large computational cost that arises from the discretization of the target correlation us-  
349 ing a low-rank expansion based on the integral representation of spherical Bessel functions.  
350 Moreover, we formally showed how to regularize the ensuing ill-posed inverse problem. Our  
351 results demonstrated that it is possible to obtain approximate diffuse fields in enclosed rooms  
352 even at frequencies below the Schroeder limit by driving correlated speakers in an optimal  
353 way. Also, we found that there is a limitation in the quality of the approximation that  
354 strongly depends on the number of speakers and the frequencies of interest. As frequency  
355 increases a larger number of speakers is needed to maintain a given level of error in the  
356 diffuse field approximation. A direction for future work is to study the influence of speaker  
357 location on the approximation error. Furthermore, it is possible to devise optimization al-  
358 gorithms to find such locations. Also, incorporating uncertainty in boundary conditions,  
359 material properties, etc. in the optimization formulation would be highly desirable.

360 **ACKNOWLEDGMENTS**

361 This work was supported by the Laboratory Directed Research and Development pro-  
362 gram at Sandia National Laboratories, a multimission laboratory managed and operated by  
363 National Technology and Engineering Solutions of Sandia LLC, a wholly-owned subsidiary of  
364 Honeywell International Inc. for the U.S. Department of Energy's National Nuclear Security  
365 Administration under Contract No. DE-NA-0003525.

366 **REFERENCES**

- 367 <sup>1</sup>M. Schroeder. Die statistischen Parameter der Frequenzkurven von großen Räumen. *Acus-*  
368 *tica*, 4:594–600, 1954.
- 369 <sup>2</sup>M. R. Schroeder. Statistical parameters of the frequency response curves of large rooms.  
370 *J. Audio Eng. Soc.*, 35(5):299–306, 1987.
- 371 <sup>3</sup>H. Kuttruff. *Room Acoustics*. Spon Press, 5<sup>th</sup> edition, 2009.
- 372 <sup>4</sup>T. J. Schultz. Diffusion in reverberation rooms. *J. Sound Vibr.*, 16(1):17–28, 1971.
- 373 <sup>5</sup>P. A. Larkin and D. O. Smallwood. Control of an acoustical speaker system in a reverberant  
374 chamber. Sandia Technical Memo SAND2003-3008C, Sandia National Laboratories, 2003.
- 375 <sup>6</sup>F. W. Grosveld and S. A. Rizzi. Controlled reverberant acoustic excitation capabilities at  
376 NASA Langley Research Center. 43rd AIAA Aerospace Sciences Meeting, AIAA-2005-  
377 0421, January 10-13, 2005.
- 378 <sup>7</sup>C. Maury and T. Bravo. The experimental synthesis of random pressure fields: Practical  
379 feasibility. *J. Acoust. Soc. Am.*, 120:2712–2723, 2006.

- 380 <sup>8</sup>M. Alvarez Blanco, P. Van Vlierberghe, M. Rossetti, K. Janssens, B. Peeters, and  
381 W. Desmet. Pre-test analysis to reproduce random pressure fields with multi-channel  
382 acoustic control. *Mech. Syst. Signal Proc.*, 163(May 2021):108103, 2022.
- 383 <sup>9</sup>S. J. Elliott and J. Cheer. Modeling local active sound control with remote sensors in  
384 spatially random pressure fields. *J. Acoust. Soc. Am.*, 137(4):1936–1946, 2015.
- 385 <sup>10</sup>S. Zhao, Q. Zhu, E. Cheng, and I. S. Burnett. A room impulse response database for  
386 multizone sound field reproduction (1). *J. Acoust. Soc. Am.*, 152(4):2505–2512, 2022.
- 387 <sup>11</sup>A.G. de Miguel, M. Alvarez Blanco, E. Matas, H. Bériot, J. Cuenca, O. Atak, K. Janssens,  
388 and B. Peeters. Virtual pre-test analysis for optimization of multi-channel control strategies  
389 in direct field acoustic testing. *Mech. Syst. Signal Proc.*, 184:109652, 2023.
- 390 <sup>12</sup>C. Van Hoorickx and E. P. B. Reynders. Numerical realization of diffuse sound pressure  
391 fields using prolate spheroidal wave functions. *J. Acoust. Soc. Am.*, 151(3):1710–1721,  
392 2022.
- 393 <sup>13</sup>R. V. Waterhouse. Statistical properties of reverberant sound fields. *J. Acoust. Soc. Am.*,  
394 43(6):1436–1444, 1968.
- 395 <sup>14</sup>F. Jacobsen. *The diffuse sound field: Statistical considerations concerning the reverberant*  
396 *field in the steady state*. Acoustics Laboratory, Technical University of Denmark, 1979.
- 397 <sup>15</sup>B. Rafaely. Spatial-temporal correlation of a diffuse sound field. *J. Acoust. Soc. Am.*,  
398 107(6):3254–3258, 2000.
- 399 <sup>16</sup>M. Grigoriu. *Stochastic Systems: Uncertainty Quantification and Propagation*. Springer  
400 Science & Business Media, 2012.

- 401 <sup>17</sup>F. Jacobsen and T. Roisin. The coherence of reverberant sound fields. *J. Acoust. Soc.*  
402 *Am.*, 108(1):204–210, 2000.
- 403 <sup>18</sup>H. Néglise and J. Nicolas. Characterization of a diffuse field in a reverberant room. *J.*  
404 *Acoust. Soc. Am.*, 101(6):3517–3524, 1997.
- 405 <sup>19</sup>P. M. Morse and K. U. Ingard. *Theoretical Acoustics*. Princeton University Press, 1986.
- 406 <sup>20</sup>F. Ihlenburg. *Finite Element Analysis of Acoustic Scattering*. Springer, 1998.
- 407 <sup>21</sup>L. Demkowicz. Asymptotic convergence in finite and boundary element methods: Part 1:  
408 Theoretical results. *Comput. Math. Appl.*, 27(12):69–84, 1994.
- 409 <sup>22</sup>F. W. J. Olver, D. W. Lozier, R. F. Boisvert, and C. W. Clark, editors. *NIST Handbook*  
410 *of Mathematical Functions*. Cambridge, 2010.
- 411 <sup>23</sup>G. H. Golub and C. F. Van Loan. *Matrix Computations*. Johns Hopkins University Press,  
412 Baltimore, 4<sup>th</sup> edition, 2013.
- 413 <sup>24</sup>P. C. Hansen. Analysis of discrete ill-posed problems by means of the L-curve. *SIAM*  
414 *Review*, 34(4):561–580, 1992.
- 415 <sup>25</sup>P. C. Hansen. *Discrete Inverse Problems: Insight and Algorithms*. SIAM, 2010.
- 416 <sup>26</sup>M. Alnæs, J. Blechta, J. Hake, A. Johansson, B. Kehlet, A. Logg, C. Richardson, J. Ring,  
417 M. E. Rognes, and G. N. Wells. The FEniCS project version 1.5. *Archive of Numerical*  
418 *Software*, 3(100), 2015.
- 419 <sup>27</sup>C. F. Eyring. Reverberation time in “dead” rooms. *J. Acoust. Soc. Am.*, 1(2A):217–241,  
420 1930.